Bull Volcanol (2011) 73:1353–1368
DOI 10.1007/s00445-011-0486-8

RESEARCH ARTICLE

The ~4-ka Rungwe Pumice (South-Western Tanzania): a wind-still Plinian eruption

Karen Fontijn · Gerald G. J. Ernst · Costanza Bonadonna · Marlina A. Elburg · Evelyne Mbede · Patric Jacobs

Received: 26 August 2010 / Accepted: 16 March 2011 / Published online: 6 May 2011

Abstract The ~4-ka trachytic Rungwe Pumice (RP) deposit from Rungwe Volcano in South-Western Tanzania is the first Plinian-style deposit from an African volcano to be closely documented focusing on its physical characterization. The RP is a mostly massive fall deposit with an inversely graded base. Empirical models suggest a maximum eruption column height H_T of 30.5–35 km with an associated peak mass discharge rate of $2.8–4.8\times10^8$ kg/s. Analytical calculations result in H_T values of 33±4 km (inversion of TEPHRA2 model on grain size data) corresponding to mass discharge ranging from 2.3 to 6.0×10^8 kg/s. Lake-core data allow extrapolation of the deposit thinning trend far beyond onland exposures. Empirical fitting of thickness data yields volume estimates between 3.2 and 5.8 km^3 (corresponding to an erupted mass of $1.1–2.0\times10^{12}$ kg), whereas analytical derivation yields an erupted mass of 1.1×10^{12} kg (inversion of TEPHRA2 model). Modelling and dispersal maps are consistent with nearly no-wind conditions during the eruption. The plume corner is estimated to have been ca. 11–12 km from the vent. After an opening phase with gradually increasing intensity, a high discharge rate was maintained throughout the eruption, without fountain collapse as is evidenced by a lack of pyroclastic density current deposits.

Keywords Rungwe · Tanzania · Plinian eruptions · Physical characterization · Eruptive parameters · Wind-free conditions · Trachyte

Editorial responsibility: P. Delmelle

K. Fontijn (✉) · G. G. J. Ernst · M. A. Elburg · P. Jacobs
Department of Geology and Soil Science, Ghent University,
Krijgslaan 281/S8,
9000 Ghent, Belgium
e-mail: Karen.Fontijn@UGent.be

C. Bonadonna
Section des sciences de la Terre et de l'environnement,
Université de Genève,
Rue des Maraîchers 13,
1205 Geneva, Switzerland

E. Mbede
Ministry of Communication, Science and Technology,
PO Box 2645, Dar es Salaam, Tanzania

Introduction

Plinian eruptions are among the most catastrophic volcanic events, but have rarely been documented in detail for African volcanoes despite the known existence of major volcanoes and calderas of Quaternary age (e.g. Menengai and Longonot, Kenya; Kilimanjaro and Meru, Tanzania; Alid, Eritrea; Siebert et al. 2011). Most studies are restricted to observations of tephra layers in lakes of the East African Rift System, often used for palaeoclimatological reconstructions (e.g. Barker et al. 2003, 2007; Barry et al. 2002; Johnson et al. 2002; Thevenon et al. 2002). An overview of some widespread known Quaternary tephra layers in Africa is given by Pyle (1999).

Rungwe Volcano in South-Western Tanzania belongs to the Rungwe Volcanic Province (RVP), part of the East African Rift System (Fig. 1, e.g. Delvaux 2001; Delvaux et al. 1992; Ebinger et al. 1989, 1993; Ring et al. 1992). The spatial relationship among tectonic rifting lineaments, larger volcanoes and numerous smaller vent constructs has been analysed by Fontijn et al. (2010a). The regional stratigraphy of volcanic deposits was first examined by Harkin (1960). The detailed Holocene eruptive history of Rungwe was recently studied by Fontijn et al. (2010b), who showed that Rungwe has had at least eight moderate- to large-scale

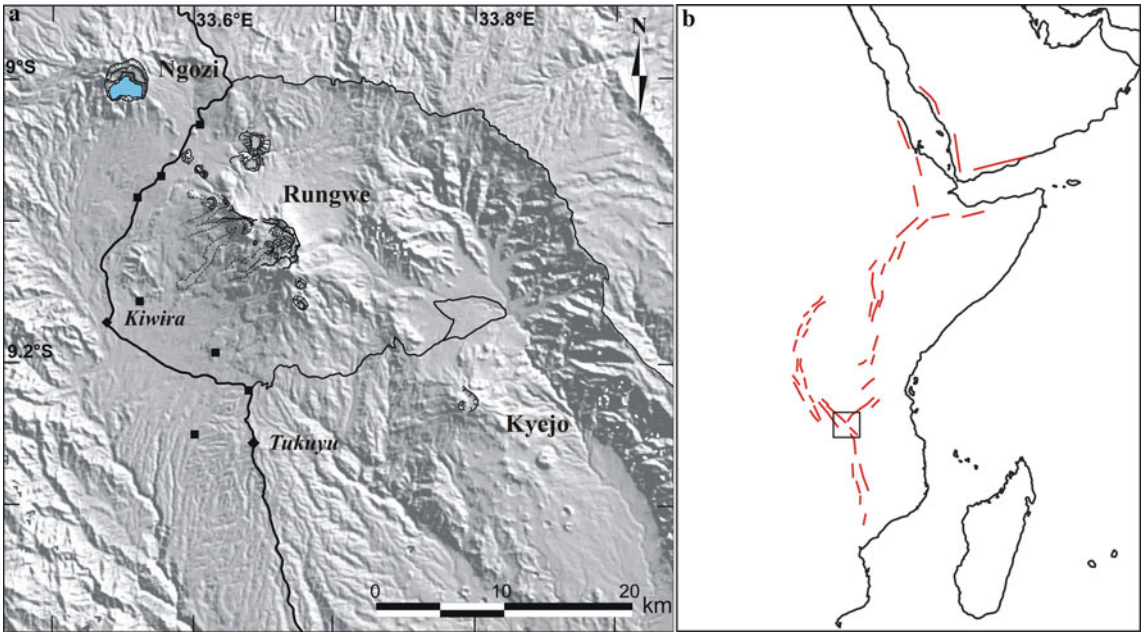

Fig. 1 **a** Shuttle Radar Topography Mission shaded relief Digital Elevation Model at 3 arcsecond (~90 m) resolution for the RVP region (USGS 2006) showing three composite volcanoes: Ngozi, Rungwe and Kyejo. Ngozi holds a caldera lake. Main roads are indicated with *full lines*; *thick line* indicates the only paved road in the region. Villages with more than 3,000 people (United Republic of Tanzania 2002) are indicated with *black squares*. *Diamonds* show two main commercial centres, Tukuyu and Kiwira. Mbeya city (not on map) is located ca. 15 km North-West of Ngozi. **b** Sketch of East Africa, with major East African Rift System faults indicated with *red lines*. *Box* indicates RVP location, corresponding to **a**

explosive eruptions in the last ~4,000 years. The most voluminous one was the ca. 4-ka Plinian-style Rungwe Pumice (RP) eruption. The RP has a trachytic composition. Well before the RP eruption, Rungwe volcano was affected by a sector collapse that generated a debris avalanche (Fontijn et al. 2010b). This sector collapse resulted in the formation of a summit crater depression ca. 5 km in diameter, subsequently filled by post-collapse cones and domes. In this paper, we focus on physical characterization of the RP deposit. This RP study documents a remarkable African volcanic eruption: (1) the isopach and isopleth maps suggest nearly wind-free eruptive conditions; and (2) there is no evidence for associated pyroclastic density current (PDC) deposits.

The RP is the very first Quaternary Plinian-style deposit to be closely documented on the African continent. Rungwe is a dormant volcano; the local population has no recollection of historical eruptive activity. Rungwe has, however, been regularly active throughout the late Holocene. All existing evidence points to a very active volcano with typical repose times of a few hundreds to a thousand years, separating violent strombolian to Plinian-style explosive eruptions (Fontijn et al. 2010b). Apart from the risk associated with pyroclastic density currents, Rungwe, the foothills of which are densely populated and which is not monitored, poses a similar threat from extensive tephra fallout, as was the case at Mt. Pinatubo before it erupted in 1991 (e.g. Newhall and Punongbayan 1996). Over two million people, the majority dependent on agriculture, live in the region of Mbeya in which the RVP is located, with the city of Mbeya located ca. 15 km North-West of Ngozi volcano (Fig. 1a). The district of Rungwe alone, with nearly all villages located within ca. 20 km from the volcano, houses more than 300,000 people (United Republic of Tanzania 2002). The main commercial centre of the Rungwe district is Tukuyu town (Fig. 1a).

The Rungwe Pumice

Stratigraphy

During three field missions between September 2007 and October 2008, the RP deposit was identified in 101 locations, mostly based on macroscopic observations, and in some cases on geochemical data (Fontijn et al. 2010b). The RP is a thick widely dispersed pumice fall deposit that can be traced in field outcrops over an area of >1,500 km^2. The majority of studied outcrops are located South of the volcano. In general, however, studied outcrops are well distributed throughout the RVP region.

Distal exposures are lacking except in Lake Malawi (in Tanzania usually referred to as Lake Nyasa) where at least seven sediment cores taken in the northern lake basin, on

average 115 km South-South-East of Rungwe, reveal a ca. 4,000–4,500 cal BP ash horizon that can be correlated with the RP and that in some cases contains small pumice lapilli (Barker et al. 2007; Barry et al. 2002; Williams et al. 1993). The reported ash bed thickness varies between cores from "discrete ash layers" (Johnson et al. 2002) to "cm-scale" beds (Barker et al. 2007; Barry et al. 2002), and exceptionally up to 30 cm (Barry et al. 2002). The thickness of the ash bed, sometimes mixed with lake sediment, varies depending on lake floor topography and is in some locations influenced by reworking after deposition (Sylvia Barry, personal communication 2010). Based on reported thickness data (Barker et al. 2007; Barry et al. 2002; Williams et al. 1993), the exceptional 30-cm thickness reported by Barry et al. (2002) is likely the result of secondary reworking, and the most likely depositional thickness in the Northern Lake Malawi basin is on the order of a few centimetres. The bed in some cores contains small pumice lapilli (Barry et al. 2002; Williams et al. 1993), and we assign a thickness of 3± 2 cm 115 km South-South-East of Rungwe.

Identification of the Rungwe Pumice was largely based on recognition of diagnostic features and/or lateral tracing in the field. The RP can be relatively easily distinguished from other-mostly younger-deposits, on the basis of its thickness and some distinctive features, e.g. the presence of free haüyne crystals. The deposit is most easily recognised South of Rungwe where it occurs at the near-surface (i.e. immediately underneath the current soil), whereas it is usually covered by younger deposits to the North of Rungwe. The RP generally occurs as a white to cream-coloured lithic-poor pumice fall deposit, showing reverse grading at the lowermost 10–15% (occasionally 30%; Fig. 2). The deposit base consists of coarse ash to small pumice lapilli, gradually coarsening upwards to the massive part of the deposit which shows very little grading itself. Reverse grading at the deposit base here suggests a gradual increase in intensity during the initial phase of the eruption. More detailed descriptions of the deposit can be found in Fontijn et al. (2010b). Despite the good coverage of studied outcrops, even within 10 km from the summit no PDC deposits were found associated with the RP: it thus seems to occur only as a fall deposit.

Spatial distribution

In most locations, the primary thickness of RP could be measured as well as maximum pumice (MP) and maximum lithic (ML) size. MP and ML were calculated as the geometric mean of the five largest pumice and lithic clasts, respectively, at each location (IAVCEI Commission on Tephra Hazard Modelling 2006; http://www.ct.ingv.it/Progetti/Iavcei/report1.htm). The area over which the largest clasts were selected spanned the entire deposit thickness over a width in the order of 1 m. Thickness, MP and ML data were used to construct isopach and isopleth maps (Fig. 3a–c). All three maps show nearly circular contour patterns indicating nearly wind-free eruptive conditions. The vent location cannot yet be constrained by the isopach and isopleth maps. We thus locate the vent centrally in the summit depression of Rungwe (Fig. 3). Currently, maximum thickness documented is 3.50 m at 12.5 km to the South-East of the centre of the Rungwe summit depression. Detailed inspection of thickness–distance relationships suggests weak dispersion to the South-South-East/East-South-East ("Column height and wind speed" and "Plume corner position" sections). The RP is still ca. 1 m and ca. 30 cm thick at 10–17 and 28 km from the central summit region, respectively.

Grain size and componentry

Channel samples, taken over the entire deposit thickness, of up to 12 kg each were taken for grain size analyses in 59 locations where the deposit was well preserved. Outcrop KF176, located 11.7 km South-South-East of Rungwe (Figs. 2 and 3), was chosen as a type section and was sampled every ca. 15–20 cm in order to investigate temporal variations in particle sedimentation. In total, 14 samples were retrieved from this section.

Grain size analyses were carried out by manual dry sieving at half-ϕ intervals from 45 mm (−5.5ϕ) down to 63 μm (4ϕ). For fractions below 2 mm, a sieve shaker was used for 1 min only at low intensity, in order to avoid clast breakage. For most samples, the fine ash fraction <63 μm represents <2 wt%. The coarsest fraction in each sample also usually represents <1.5 wt% of the total sample mass.

Within the −5.5ϕ to 4ϕ range, most samples show a unimodal grain size distribution (GSD). Inman parameters $Md_\phi(=\phi_{50})$ and $\sigma_\phi(=(\phi_{84}-\phi_{16})/2)$, respectively the median diameter and sorting (Inman 1952), were calculated for all GSDs. The spatial distribution of Md_ϕ values with nearly circular contour lines (Fig. 4a) again suggests nearly wind-still conditions during the eruption. Figure 4b, c illustrates the distribution of Md_ϕ and σ_ϕ as a function of distance from the vent. As expected, on average, σ_ϕ decreases slightly (i.e. sorting improves) with distance whereas Md_ϕ increases (i.e. deposit becomes finer). Figure 4d shows a plot of σ_ϕ vs. Md_ϕ values: σ_ϕ is systematically <2.0, i.e. consistent with RP being a well-sorted fall deposit (Cas and Wright 1987; Walker 1971).

The variations of grain size data, i.e. Md_ϕ, σ_ϕ, MP and ML at the KF176-type locality (Fig. 5a, b), are overall consistent with each other: lower Md_ϕ values (i.e. median grain size becoming coarser) are reflected in higher MP and ML values. Apart from the clear reverse grading in the lower 50 cm of the deposit, grain size variations higher in the section are more subtle and consistent with the massive appearance of the deposit in the field. Sorting deteriorates slightly (i.e. higher σ_ϕ) from base to top.

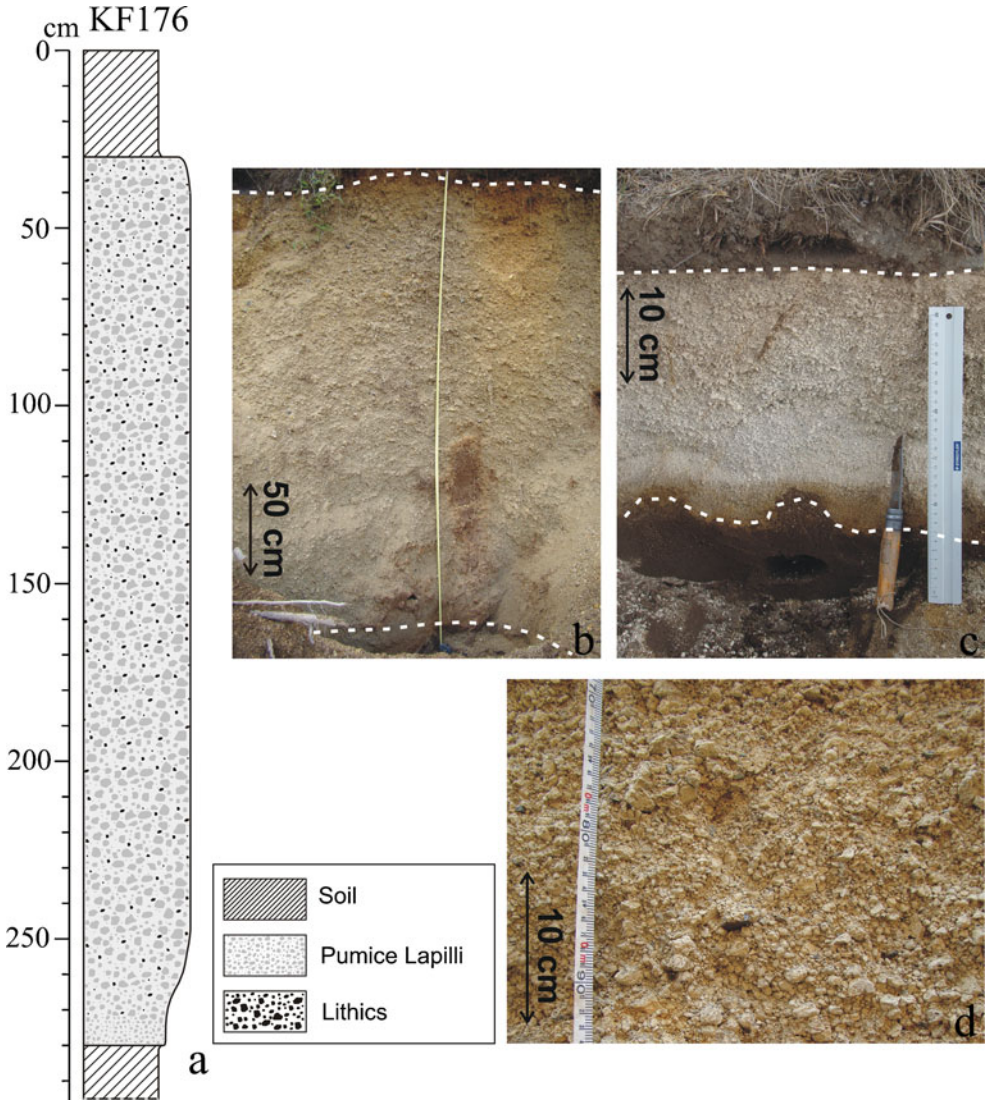

Fig. 2 **a** Representative lithology of RP in type section KF176 located 11.7 km South-South-East from the centre of the Rungwe summit crater depression. The deposit is ca. 2.5 m thick at this location. **b** Field photo of type locality KF176. **c** Field photo of 30-cm-thick RP deposit located 28.1 km East-North-East from Rungwe. Strong reverse grading at base and weak normal grading towards top of RP are evident. *Dashed lines* in **b** and **c** indicate soil–pumice breccia boundaries. **d** Close-up of representative outcrop at 15.7 km South-South-East from Rungwe and displaying typical RP appearance, i.e. a lithic-poor, cream-coloured pumice lapilli breccia

For the 14 samples for type locality KF176, fractions down to 1 mm (0φ) were separated manually into distinct components to investigate vertical variations in, for example, lithic-fragment content. For most samples, the analysed fraction represents more than 85 wt% of the total sample mass. Four different components were identified: (1) dominant cream-coloured pumices, (2) subordinate banded to greyish pumices interpreted to reflect a slightly more mafic magma composition than the dominant pumice fraction, (3) lithic fragments (dominantly trachytic lava with subordinate syenite; Fontijn et al. 2010b) and (4) free crystals (mainly alkali feldspar, with subordinate amounts of haüyne, biotite, clinopyroxene and Fe–Ti oxides). Variations in componentry through the RP type section KF176 have been investigated for each grain size fraction separately. The banded/grey pumice fraction generally represents <1 wt%. Figure 5c illustrates the upsection variations in total analysed lithic-fragment and free crystal content for all fractions down to 1 mm. Apart from the anomalous second lowermost value, the lithic content generally follows the same trend as ML values (Fig. 5b), except for a sharp peak in the second lowermost interval of the deposit and a more pronounced increase in the top 20% of the deposit section compared to ML values. In the lower 20% of the deposit section, the sharp peak in lithic wt% is present for all grain size fractions and is concomitant with the rapid increase in median grain size (see also the sudden increase in MP, Fig. 5b). The free crystal content closely follows the generally coarsening-upward trend of Md_{ϕ}, including the subtle decrease again at the very top of the deposit.

Total grain size distribution

The total grain size distribution (TGSD) for RP was estimated using four different techniques: (1) Voronoi tessellation (Bonadonna and Houghton 2005), (2) volume and mass calculation of isomass (mass/area) maps for each

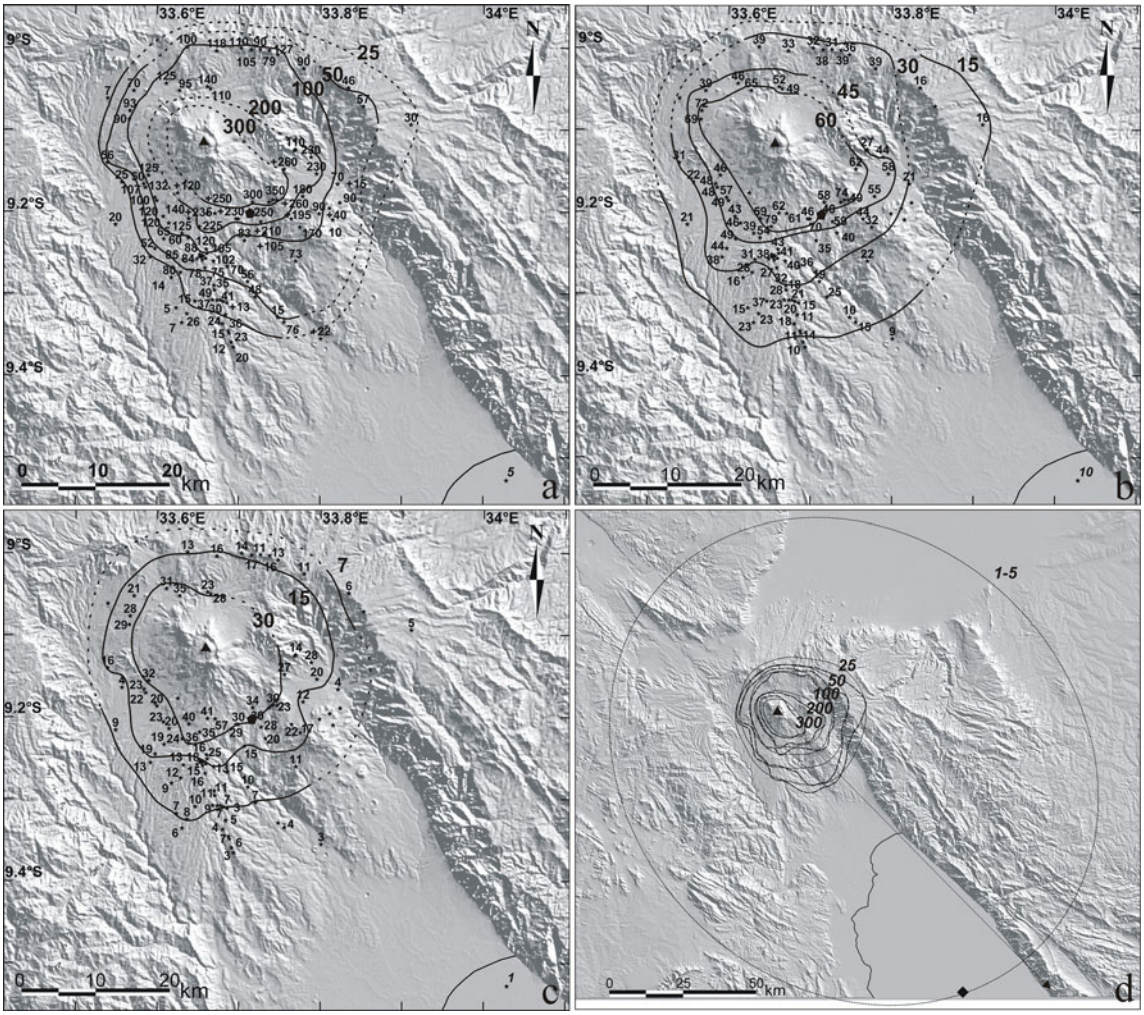

Fig. 3 **a** Isopach map for RP; values in cm. **b** Isopleth map of MP values, given in mm. **c** Isopleth map of ML values, given in mm. Parts of isopach and isopleth contours which are not well constrained by field data are indicated with *dashed lines*. *Values in italics* refer to less well-constrained estimates or non-primary thicknesses. The data point in Northern Lake Malawi (*border indicated with solid line*) is a rough estimate. Vent location is tentatively indicated by *black triangle placed centrally* on Rungwe summit area. *Pentagon symbol* South-South-East of Rungwe summit indicates location of type section KF176. **d** Isopach map of RP including data point from Lake Malawi (*diamond*) with 1–5-cm isopach inferred with method of ellipses (Sulpizio 2005). Isopach contours from field data **a** are *drawn in dashed lines* and approximated by elliptical contours (*full lines*) with mean eccentricity of 0.52. Contour values represent deposit thickness in cm

interval, (3) semi-analytical modelling of mass/area values per ϕ interval using TEPHRA2 dispersal model in inverse mode (Bonadonna et al. 2005; Connor and Connor 2006; Volentik et al. 2010), (4) mass-weighted averaging of individual GSDs (Walker 1981). The resulting TGSDs and their Inman parameters Md_ϕ and σ_ϕ are presented in Fig. 6 and Table 1.

The Voronoi tessellation method requires the definition of a zero deposit accumulation limit. Two constraints are currently useful for defining this limit: (1) sediment cores in Northern Lake Malawi, 115 km South-South-East of Rungwe (Barker et al. 2007; Barry et al. 2002; Johnson et al. 2002, 2010; Williams et al. 1993; see also "Stratigraphy" section), contains RP ash, whereas (2) a core in Lake Rukwa, drilled 120 km North-West of Rungwe (Thevenon et al. 2002), does not contain any tephra layers that could be correlated to RP (Fontijn et al. 2010b). Furthermore, the isopach and isopleth maps (Fig. 3) are consistent with one another, and indicate only a weak influence of wind upon ejecta dispersal. Lake Malawi core data (Barker et al. 2007; Barry et al. 2002; Johnson et al. 2002, 2010; Williams et al. 1993) suggest that fine ash of the RP eruption must have been dispersed further than 115 km South-South-East. As mentioned in "Stratigraphy" section, the most likely RP thickness in the Northern Lake Malawi basin is 3±2 cm.

The zero accumulation line was chosen as concentric with the estimated 3±2 cm isopach (Fig. 3d; "Erupted volume" section) and at distances of ca. 160 km South-East

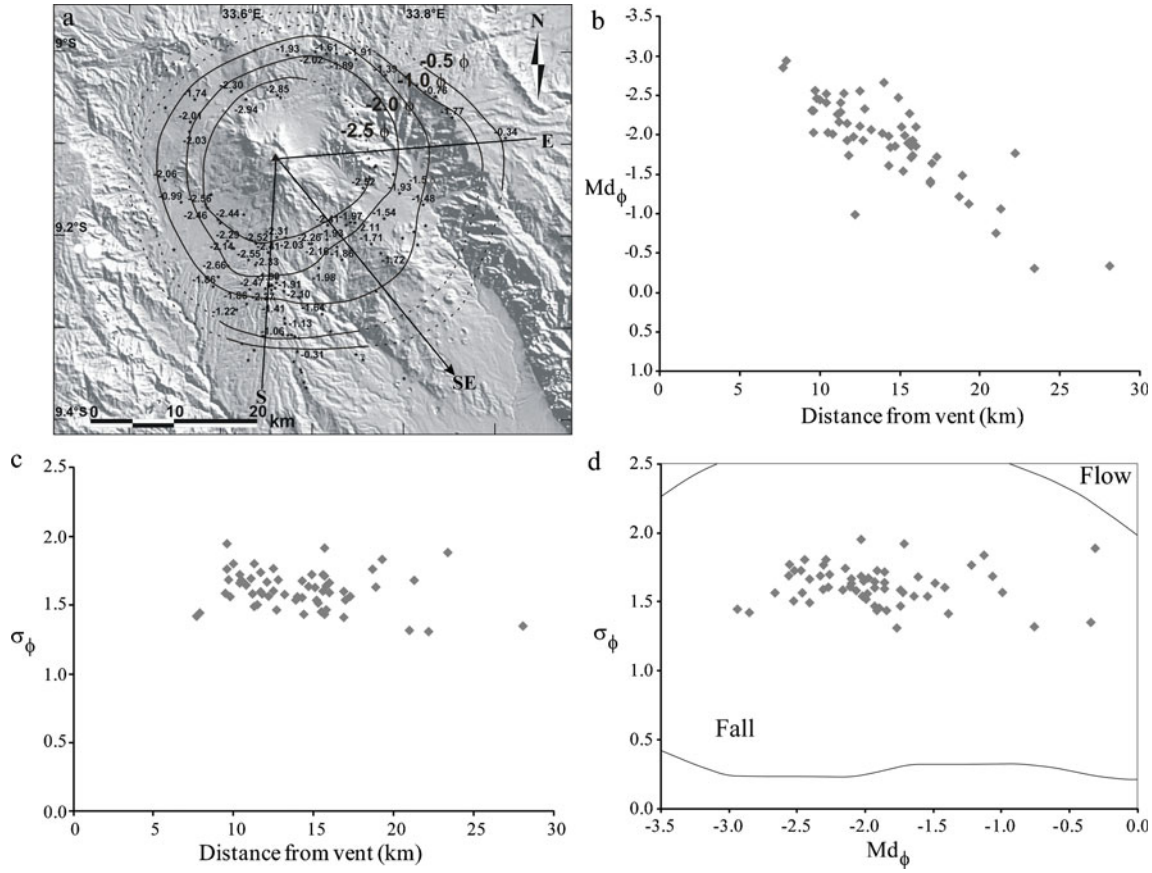

Fig. 4 **a** Iso-Md$_\phi$ map of RP deposit showing nearly circular contours. Three axes along, which accumulation ("Plume corner position" section) was investigated, are also indicated. South-Eastern axis corresponds to the dispersal axis. Plot of Md$_\phi$ (**b**) and σ_ϕ (**c**) values in function of distance from the vent (i.e. centre of summit region). **d** Plot of Md$_\phi$ vs. σ_ϕ indicating fallout origin of the deposit; pyroclastic fall and flow fields after Walker (1971)

and ca. 100 km North-West from Rungwe. Volentik et al. (2010) demonstrate that the choice of the zero accumulation line necessary for the Voronoi technique does not significantly influence the TGSD estimate. Individual GSDs of 59 samples were weighted by Voronoi cell area and mass/area values for each sample location. The mass/area value for each sample location was estimated by multiplying the deposit thickness with the average bulk deposit density.

The bulk density was derived by weighing a known volume of several samples taken from representative locations. Thirty different laboratory measurements on samples with a representative GSD with maximum clast size on the order of −5ϕ yield a very reproducible average bulk density of 343±1 kg/m^3. This value is exceptionally low compared to previously published bulk density values for Plinian fall deposits (e.g. Bursik et al. 1992; Hildreth and Drake 1992; Volentik et al. 2010) which can be readily accounted for by the low pumice density. Measurements of a set of 100 test clasts from type section KF176, in the size range of −4ϕ to −5ϕ, yielded densities on the order of 400–450 kg/m^3, corresponding to vesicularities of 0.80–0.83 (glass density 2,300 kg/m^3). High vesicularities (and hence low densities) for trachytic pumices on the order of 0.80–0.85 and even up to 0.90 as compared to typical values for rhyolitic pumices (0.64–0.76) have also been reported by Polacci et al. (2003, 2004). The use of an average bulk density for the entire deposit is reasonable in this case because variations in GSDs between samples are relatively small, arguably because only the proximal-to-medial part of the deposit is exposed.

From total mass/area values from each location and individual GSDs, isomass maps can be constructed for each grain size class, similar to the isopach map for the entire deposit (Fig. 3a). From such isomass maps, volumes can be estimated using the exponential integration method from Pyle (1989). Here, isomass contour values are converted to thickness with the average bulk density (because density values per grain size fraction are lacking), and the minimum volume of each grain size fraction is estimated. As individual GSDs contain low amounts of fine ash, mass/area data for the +4ϕ fraction are scarce, and no isomass map could be constructed for this grain size. Therefore, the

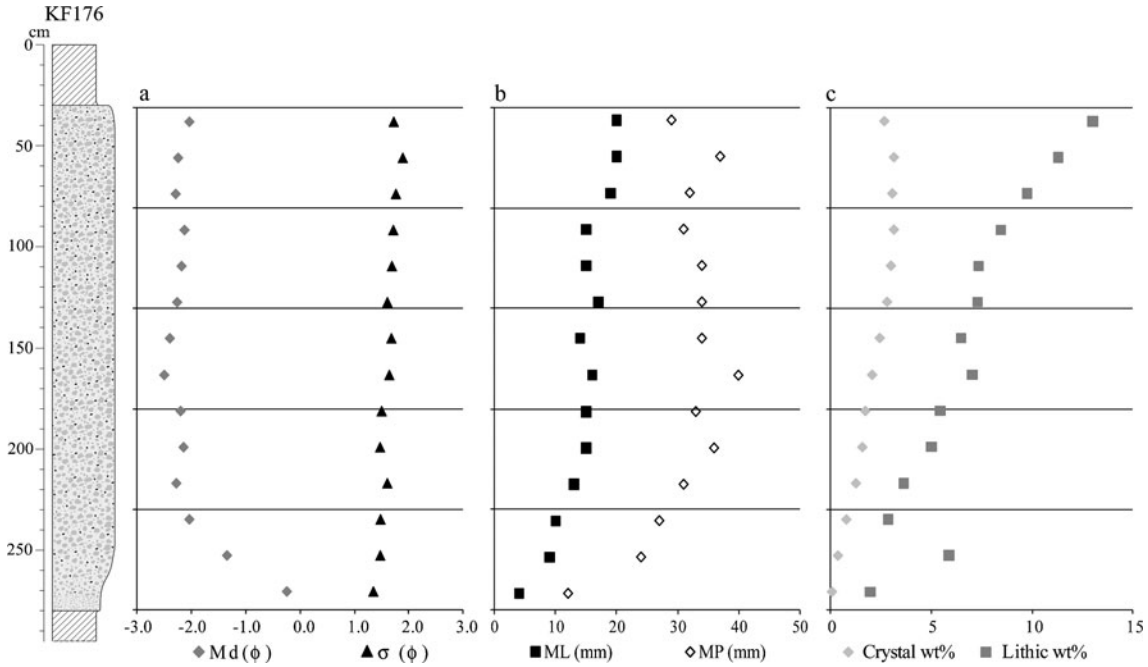

Fig. 5 Variation of **a** Md_ϕ and σ_ϕ, **b** MP and ML, and **c** wt% of lithics and free crystals in fraction down to 0φ within RP deposit at KF176 type locality; log legend in Fig. 2. Md_ϕ values show reverse grading at base with a weak trend of normal grading (i.e. Md_ϕ values becoming slightly larger) towards the top of the deposit. Sorting gradually decreases upwards (σ_ϕ becoming larger). MP and ML values were determined in the lab and confirm the general coarsening upwards trend. In the middle third part of the deposit, some rather subtle grain size (Md_ϕ, MP and ML) variations occur. Coarsening upwards trend is also confirmed by increasing wt% of dense fragments (both lithics and free crystals)

TGSD resulting from this technique is likely biased towards the coarse fractions, which is evident from Fig. 6 and the Md_ϕ of −2.4.

Mass/area values per grain size fraction can also be used as input for inversion modelling with TEPHRA2, an analytical model based on the advection–diffusion equation (Bonadonna et al. 2005; Connor and Connor 2006; Volentik et al. 2010). With inversion modelling of the observed values of tephra accumulation (mass/area in each sample location), it is possible to find a set of eruptive parameters (erupted mass and column height) that best describes the observed deposit. The inversion technique uses the downhill simplex algorithm, minimising the error between measured and estimated tephra accumulation (mass/area) in each

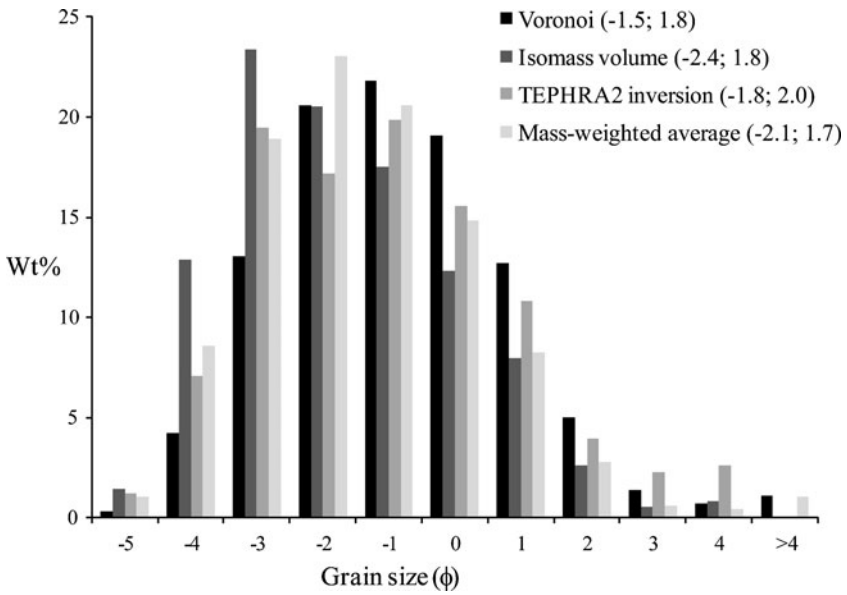

Fig. 6 TGSDs of RP deposit calculated with four different methods from 59 sample locations: (1) Voronoi tessellation with zero accumulation line concentric with the ca. 3-cm isopach at a distance of 160 km South-East and ca. 100 km North-West from Rungwe ("Erupted volume" section). Individual sample GSDs were weighted by mass/area value and area of assigned Voronoi cell. (2) Volume calculations of isomass maps for each 1-phi interval. (3) TEPHRA2 inversion on mass/area values per grain size (ϕ intervals). (4) Mass-weighted average after Walker (1981). *Numbers between brackets in legend* represent Md_ϕ and σ_ϕ for each TGSD, respectively

Table 1 Summary of modelled parameters with indication of different methods used and their respective results

Eruption parameter	Method	Result	
		Md_ϕ	σ_ϕ
TGSD	Voronoi tesselation[1]	−1.5	1.8
	Isomass maps per grain size	−2.4	1.8
	TEPHRA2 inversion[2] on mass/area per grain size fraction	−1.8	2.0
	Mass-weighted average	−2.1	1.7
Erupted volume	One segment, exponential fit[3]	2.2 km^3	
	Two segments, exponential fit[3] (Malawi 1–5 cm)	3.2–5.6 km^3	
	Power-law[1] (Malawi 1–3 cm)	3.3–5.8 km^3	
	Power law[1] (Malawi 5 cm)	8.5 km^3	
Erupted mass		$1.1–2.0\times10^{12}$ kg	
	TEPHRA2 inversion[2] on total mass/area	1.1×10^{12} kg	
Plume corner	Maximum accumulation[4], South-Eastern axis	12 km	
	Maximum accumulation[4], Southern axis	10.5 km	
	Maximum accumulation[4], Eastern axis	8.5–11.5 km	
Classification	VEI[5]	5	
	Magnitude[6]	5–5.3	

TGSD total grain size distribution, Md_ϕ median ($\phi50$), σ_ϕ sorting $((\phi_{84}-\phi_{16})/2)$, *VEI* Volcanic Explosivity Index

See text for details on applied methodology. Malawi 1, 3 or 5 cm indicates applied thickness in Lake Malawi location (115 km South-South-East)

References for applied methods:

[1] Bonadonna and Houghton (2005)

[2] Bonadonna et al. 2005; Connor and Connor 2006; Volentik et al. 2010

[3] Pyle (1989), Pyle (1995)

[4] Bursik et al. (1992)

[5] Newhall and Self (1982)

[6] Pyle (2000)

location (Connor and Connor 2006). When applied to the accumulated mass in each location, a best fit for total erupted mass is found ("Erupted mass" section; Volentik et al. 2010). Here, the inversion is applied to mass/area for each ϕ interval to find an erupted mass for each interval and derive a TGSD. The inversion is not applied to the +4ϕ fraction, resulting in a TGSD that is expected to be too coarse.

Finally, standard mass-weighted averaging introduced by Walker (1981) was also applied to derive a TGSD. This technique results in a distribution that is remarkably coarse.

The TGSD estimates presented in Fig. 6 and Table 1 are representative for the medial exposed part of the deposit only because no constraints are available on the original amount of fine ash that was erupted. The Voronoi tessellation method takes the spatial distribution of the deposit into account and is only dependent on total mass/area (derived from thickness and bulk density) and not on individual GSDs in contrast to the other described methods. The TGSD estimated with the Voronoi tessellation method is therefore considered to be the most reliable with respect to the medial part of the deposit.

Eruptive parameters

Erupted volume

Estimation of the RP deposit volume is somewhat problematic because of limited availability of data in distal areas. Five isopachs could be constrained based on field data, all from the (proximal to) medial parts of the deposit, whereas at least 10–15 isopachs spanning proximal to distal regions would be necessary to better describe the thinning trend (e.g. Bonadonna and Houghton 2005; Bonadonna et al. 1998). Theoretical modelling by Bonadonna et al. (1998) showed that many deposits exhibit 3–4 exponential segments corresponding to different sedimentation regimes. Segment 0 is the result of sedimentation from the eruption column margin, whereas Segments 1, 2 and 3 are expected to result from distinct sedimentation regimes for the umbrella cloud or advected gravity current spreading near the neutral density height. Segment 1 is the result of sedimentation of coarse ash and lapilli in a turbulent regime. Segment 2 corresponds to a transitional regime,

and Segment 3 corresponds to fine ash sedimentation in a laminar regime. When sufficient proximal and distal data are available, deposit thinning can also be approximated by a power-law fit (Bonadonna and Houghton 2005), in which the thinning is described by $T = T_{pl}\ \sqrt{A}^{(-m)}$, where T is thickness in m, A the isopach area in m^2, T_{pl} the power-law coefficient and m the power-law exponent. Volume and other eruptive parameters estimates are listed in Table 1.

One segment on a log T vs. $\sqrt{A}$ plot yields a *minimum* volume (Pyle 1995) of 2.2 km^3. This one segment that can be defined based on field data corresponds to Segment 1 of Bonadonna et al. (1998), i.e. the proximal deposition of particles with high Reynolds number (coarse ash and lapilli) falling from the umbrella cloud.

The geometry of isopach contours suggests some ash dispersal towards the East-South-East/South-South-East. Based on the Lake Malawi core data, a 3±2-cm thick ash layer approximately 115 km South-South-East of Rungwe is assumed (Barker et al. 2007; Barry et al. 2002; Johnson et al. 2002, 2010; Williams et al. 1993; "Stratigraphy" and "Total grain size distribution" sections). To assign a $\sqrt{A}$ value to this data point, the empirical method of ellipses as introduced by Sulpizio (2005) is used. The mean eccentricity of medial isopachs is 0.52, and this value was also assigned to the distal ca. 3 cm isopach (Fig. 3d). With this sixth isopach, two segments on the log T vs. $\sqrt{A}$ plot can be identified (Fig. 7). Estimation of the deposit volume with the exponential method based on the six isopachs with two segments yields a value range of 3.2–5.6 km^3, i.e. ca. 50% to 150% more than the value obtained without the distal point.

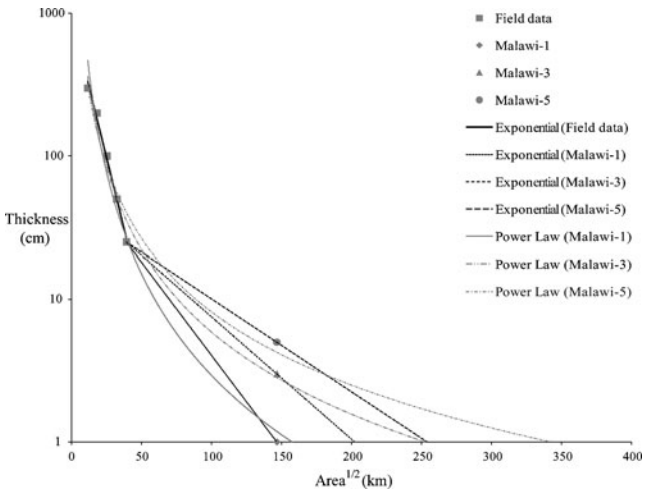

Fig. 7 Log T vs. $\sqrt{A}$ of RP deposit. Exponential fitting results in two segments. The first one is based on field data (*solid line*); a second segment can be inferred from the distal data derived from Lake Malawi cores where RP thickness is estimated at 3±2 cm (see text for details). *Malawi-1*, *-3* and *-5* indicate 1, 3 and 5 cm thickness, respectively. This thickness range provides a range of second segment slopes and therefore also a range of estimated volumes

When incorporating the distal Malawi data point, the power law fitting method (Bonadonna and Houghton 2005) can be applied (Fig. 7). The power law function fits well for Malawi point thicknesses of 1 and 3 cm, resulting in estimated volumes of 3.3 and 5.8 km^3, respectively. These estimates are consistent with the volume range obtained with the exponential fitting. For a thickness of 5 cm, the power law curve does not fit the data as well, and results in a volume of 8.5 km^3, which is likely to be an overestimate. This may lead to the conclusion that the deposit thickness at the Lake Malawi location is most likely to be in the range of 1–3 cm.

Because a clear proximal segment on the log T vs. $\sqrt{A}$ plot cannot be determined, and because currently we do not have more constraints on the ca. 3-cm isopach, a minimum volume for the RP deposit of 3.2 km^3, corresponding to a dense rock equivalent volume of 1.4 km^3 (rock density 2,300 kg/m^3), is suggested. Linear extrapolation of the medial data segment to $\sqrt{A}$=0 km suggests a maximum thickness T_0 of 9.7 m. This value is probably an underestimation as no real proximal segment(s) formed by fallout from the plume margin (Segment 0 of Bonadonna et al. (1998)) can be defined based on field data, and proximal segments should have a steeper slope than medial segments.

Erupted mass

With the estimated volume range of 3.2–5.8 km^3 and the average bulk density of 343 kg/m^3 ("Total grain size distribution" section), the total erupted mass is estimated to be $1.1–2.0\times10^{12}$ kg (Table 1). This range probably underestimates the erupted mass because the bulk density given only applies for the medial part of the deposit, of which the volume is estimated to be approximately 2.2 km^3 ("Erupted volume" section). The distal part of the deposit probably has a higher bulk density because it contains more fine ash than the medial part.

If the inversion of TEPHRA2 ("Total grain size distribution" section) is applied to the total mass/area values (kg/m^2, derived from the thickness in each location and the bulk deposit density), the best fit for the total erupted mass is constrained to 1.1×10^{12} kg which is consistent with our empirical estimations.

Column height and wind speed

The maximum eruptive column height H_T was derived with the method of Carey and Sparks (1986) based on ML isopleths, yielding a value range for H_T of 30.5–33 km and for wind speed of 2.5–8.5 m/s. Due to the irregularity in contour shapes, a range of values can be defined for each isopleth. The different isopleths yield internally consistent values (Table 2). The maximum H_T can also be estimated

Table 2 Summary of modelled column height, wind speed and associated MDR calculated with the equation from Wilson and Walker (1987)

Method	H_T	Wind speed	MDR
CS86[1], ML 8 mm	31–33 km	4–8.5 m/s	$3.0–3.8\times10^8$ kg/s
CS86[1], ML 16 mm	30.5–32.5 km	2.5–5.5 m/s	$2.8–3.6\times10^8$ kg/s
Pyle[2]	35 km	–	4.8×10^8 kg/s
TEPHRA2 inversion[3] on mass/area per grain size fraction	33±4 km	–	$2.3–6.0\times10^8$ kg/s

ML maximum lithic size, H_T eruption column height, *MDR* mass discharge rate

References for methods:

[1] CS86 Carey and Sparks (1986)

[2] Pyle (1989)

[3] Bonadonna et al. (2005), Connor and Connor (2006), Volentik et al. (2010)

using the method of Pyle (1989) in which the slope of the best-fit equation for Segment 1 on the log T vs. $\sqrt{A}$ plot (Fig. 7) is proportional to the height of the neutral buoyancy level H_B, which in turn is related to H_T (Sparks 1986). This results in a maximum H_T of 35 km which is of the same order of magnitude as the value obtained by the Carey and Sparks (1986) method (Table 2). H_T can also be constrained by TEPHRA2 inversion on individual grain size classes ("Total grain size distribution" section; Volentik et al. 2010). Inverting on RP grain size results in a range of possible values that best explain the field data of H_T 33± 4 km, consistent with the results acquired from empirical models.

The observed thinning trend of the deposit can be simulated with the strong plume model of Bonadonna and Phillips (2003) which simulates sedimentation from the base of an umbrella cloud spreading laterally from a subvertical eruption column (Fig. 8). Because the model only describes particles falling out from the base of the laterally spreading plume at the neutral buoyancy level (so excluding marginal fallout), the accumulated mass at a given distance is normalised to the mass at the plume corner, representing the transition between the subvertical convective column and the laterally spreading current in the umbrella region of the eruption column. In our field data, we assume the plume corner to be roughly located at the first data point at ca. 11.5 km distance ("Plume corner position" section). The modelled thinning trend confirms that the exposed part of the deposit (field data plotted in Fig. 8) corresponds to high-Re particles falling in the turbulent sedimentation regime from the umbrella cloud (Bonadonna et al. 1998). Best fit is associated with a wind speed of 5 m/s and a plume height of 20 km, which is not considered representative due to the large sensitivity of this model to the TGSD, which, in this case, probably lacks of the fine fraction (Volentik et al. 2010).

Mass discharge rate

The mass discharge rate (MDR) can be estimated from the inferred H_T ("Column height and wind speed" section, Table 2) with the equation of Wilson and Walker (1987): $H_T=0.236\times M_0^{1/4}$ with M_0 the MDR in kg/s. This equation applies to a circular vent (or an elongated vent of which the length is considerably shorter than the column height) and eruption temperatures of 1,120 K, expected to apply to trachytic magmas like the RP one (e.g. Di Matteo et al. 2004). Given that the plume height derived from empirical methods is based on the distribution of the maximum clasts, it has to be considered as a maximum plume height. As a result, the associated MDR has to be considered as a peak MDR (i.e. H_T 30.5–35 km and MDR $2.8–4.8\times10^8$ kg/s). Nonetheless, the MDR associated with the plume height range derived from the TEPHRA2 inversion can be considered as an average MDR because it is based on the TGSD at each location (i.e. H_T 29–37 km and MDR $2.3–6.0\times10^8$ kg/s).

Plume corner position

Because the RP eruption happened during nearly wind-still conditions, we can apply the method of Bursik et al. (1992) to estimate the corner position of the eruption plume by investigating the accumulation of grain size classes with distance from the vent. The accumulation per unit distance (kg/m), estimated by multiplying accumulation per unit area (kg/m^2) with the perimeter length of the isopach contour passing through the respective location, is plotted against the distance from the vent for each grain size class. For clarity, only one-φ intervals are used here. Because some influence of wind during the eruption is expected, we define three axes along which accumulation per unit distance can be plotted: East, South-East and South (Fig. 4a). The South-Eastern axis corresponds to the dispersal axis inferred from the RP isopach

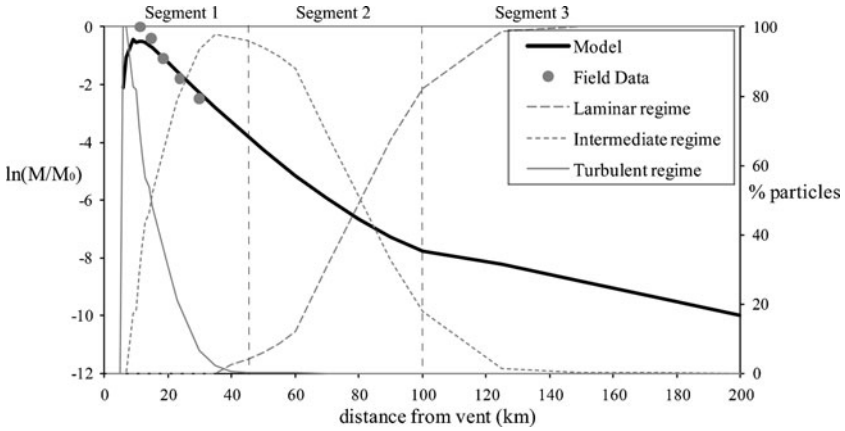

Fig. 8 Semi-logarithmic plot of plume corner-normalised accumulated mass (M/M_0, *left vertical axis*) as a function of distance along dispersal axis calculated with the strong plume model of Bonadonna and Phillips (2003). Best fit is reached for H_T 20 km and wind speed 5 m/s. Field data are indicated as *circles*. The Lake Malawi data point is not shown as the bulk density in this location is not known and should be significantly different from the bulk density of the medial part of the deposit (field data). Also shown are model-calculated percentages (*right vertical axis*) of particles falling in three different sedimentation regimes: turbulent, intermediate and laminar, according to particle Reynolds numbers

and isopleth maps (Fig. 3). This methodology has also been applied by Volentik et al. (2010) to investigate the plume corner position for the no-wind 2450 BP Pululagua BF2 deposit.

The data presented in Fig. 9 apply to the Southern axis and were fitted to fifth-order polynomials to find the distance of the accumulation maximum of each grain size class (Bursik et al. 1992). The South-Eastern and Eastern axes give similar results (Table 1). Accumulation of 32–64-mm particles follows an irregular trend along all three axes. This can be accounted for by the fact that grain size data for all particles were used, both dense lithics and pumice, and that pumices might have broken upon landing to some extent. This breakage influence is especially expected for pumices larger than ca. 3 cm (Kaminski and Jaupart 1998). 16–32-mm and 8–16-mm particles follow a general decrease in accumulation with distance from the vent. This trend has been attributed to particles falling from the plume margins rather than out of the umbrella region (Bursik et al. 1992; Volentik et al. 2010). Only along the Southern axis (Fig. 9), a clear maximum exists in the polynomial fit for the 8–16-mm class at ca. 10.5-km distance (Fig. 9). Accumulations for 4–8- to 1–2-mm particles show an increase, before reaching a maximum accumulation and then decrease again with distance from the vent. This maximum in accumulation per unit distance is associated to the plume corner position (Bursik et al. 1992). For the Eastern axis, the maximum increases slightly with decreasing particle size, from ca. 8.5 km for the 4–8-mm class to 11.5 km for the 1–2-mm class. For the Southern and South-Eastern axes, maxima for the same grain size range are not dependent on grain size and are on average 10.5 and 12 km respectively (Table 1). Based on the relation between plume corner and plume height in no-wind conditions (Bonadonna and Phillips 2003), a plume corner between 8.5 and 12 km corresponds to a plume height between 35 and 50 km. As a result, the dispersal along the South-Eastern axis is expected to be influenced by a certain degree of wind transport.

Accumulation of particles smaller than 1 mm shows a similar trend towards a maximum, followed by a decrease, and then another general increase with distance. Bursik et al. (1992) and Volentik et al. (2010) defined a secondary accumulation maximum for these finer grain sizes, but here, field data probably do not reach far enough from the vent to reveal any such secondary maximum. Accumulations of the finest particle sizes were not all fitted to a fifth-order polynomial because we feel they could indicate spurious maxima and minima in the curves.

Classification

Based on the one-segment extrapolation on the log T vs. $\sqrt{A}$ plot (Fig. 7, "Erupted volume" section), a near-vent deposit thickness T_0 or T_{max} of ca. 9.7 m is inferred. Starting from this value, the dispersal D and fragmentation index F as defined by Walker (1973) can be estimated. The value of D, ca. 2,300 km^2, is the area within a 10-cm isopach that was drawn based on extrapolation of isopachs constrained by field data (Fig. 3a). F is 12.7% and was estimated as the average of wt% values of the <1-mm fraction of three samples located close to the deposit dispersal axis and close to the 100-cm isopach (i.e. 0.1 T_{max}). With these values for D and F, the RP is unambiguously classified as a Plinian fall deposit (Walker 1973). This classification is consistent also with dispersal characteristics based on the isopach map and the classification scheme of Pyle (1989).

The estimated deposit volume range of 3.2–5.8 km^3 (Table 1) suggests that the RP eruption was a VEI 5 event (Newhall and Self 1982). The erupted mass of 1.1–2.0×

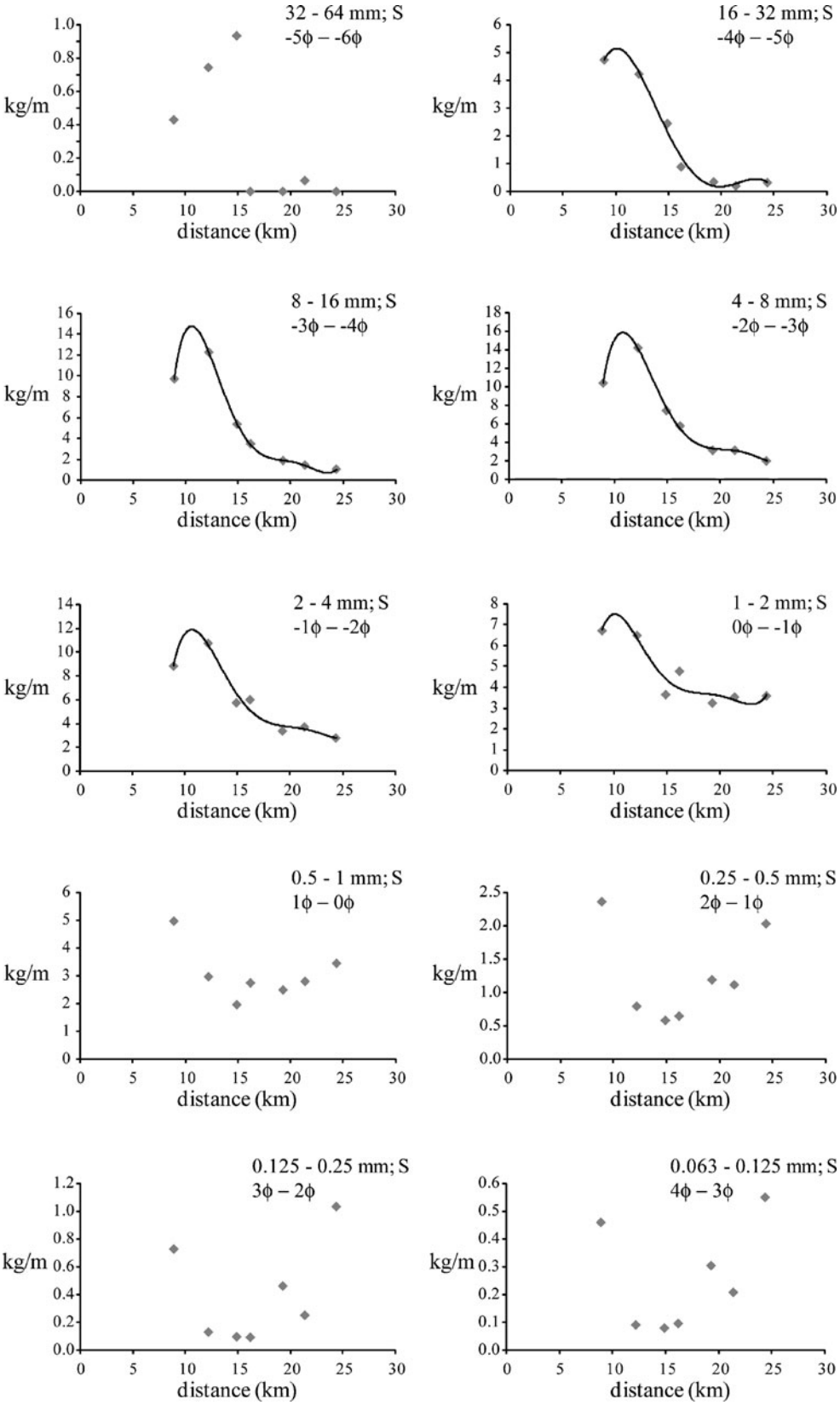

Fig. 9 Mass accumulation per unit distance (kg/m) of grain size classes >32 to >63 μm along the Southern axis (Fig. 4a). Accumulation patterns along South-Eastern and Eastern axes (Fig. 4a) are similar

10^{12} kg ("Erupted mass" section) corresponds to a magnitude 5–5.3 eruption (Pyle 2000). Figure 10 shows log T vs. $\sqrt{A}$ for RP compared with other deposits from highly explosive eruptions with similar dispersal characteristics, including the no-wind Pululagua BF2 deposit (Papale and Rosi 1993; Volentik et al. 2010).

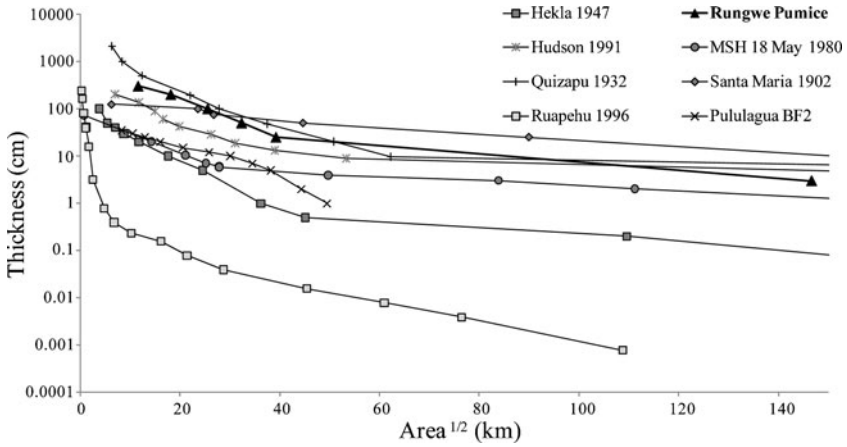

Fig. 10 Log T vs. $\sqrt{A}$ plot of RP deposit compared with thinning trends of other large explosive eruptions. References: Hekla: Thorarinsson (1954); Mount Saint Helens (*MSH*): Sarna-Wojcicki et al. (1981); Santa Maria: Williams and Self (1983); Quizapu: Hildreth and Drake (1992); Hudson: Scasso et al. (1994); Ruapehu: Bonadonna and Houghton (2005); Pululagua: Volentik et al. (2010)

Discussion

The ~4-ka RP deposit allows a remarkable case study of an eruption that took place in nearly no-wind conditions, with a slight dispersal towards the South-South-East. Despite the wide dispersal in the RVP region, it was not possible to trace the RP deposit back to the summit or into the summit crater depression, because it is covered with younger tephra deposits or thick silicic lava flow deposits. Due to the lack of RP exposures at the summit, and to the nearly wind-free conditions during the eruption, the vent location was not identified, but it has been tentatively positioned centrally in the Rungwe summit crater depression (Fig. 3). Field and grain-size data suggest that the eruption started with a relatively low intensity phase after which the intensity quickly increased to a peak which was maintained throughout most of the eruption (Fig. 5). The peak in lithic content recorded near the base of the type section is systematically found in all grain size fractions. This peak is concomitant with the intensity increase (Fig. 5) and is thus attributed to clearing of the vent, after which the mass discharge increased towards its peak rate, i.e. $2.8–4.8\times10^8$ kg/s as inferred from empirical models ("Mass discharge rate" section, Table 2).

The fact that the eruption column was sustained until the end of the eruption, and apparently no fountain collapse occurred to generate PDCs, has implications for the conduit geometry and the volatile content of the magma. The gradual increase in (dominantly trachytic) lithics in the type section KF176 (Fig. 5c) suggests a certain amount of vent widening through erosion during the eruption. This process is expected to result in an increase in MDR and associated generation of PDCs because of fountain collapse (e.g. Woods 1998). Neither a caldera nor deposits from PDCs are found, however. The estimated peak MDR range of $2.8–4.8\times10^8$ kg/s constrains inferences of the crater radius (assuming a round vent) to ca. 50–60 m (Woods 1998; Woods and Bower 1995). The estimated MDR range is near the boundary below which fountain collapse can be expected, i.e. 2.0×10^8 kg/s. Above this value, major PDCs and subsequent caldera collapse could be expected (Carey and Sigurdsson 1989). In this case, however, the pumice clast density is extremely low, i.e. of order 400–450 kg/m^3. Despite a high MDR and a moderate increase in lithic content resulting from vent widening, this extremely low pumice density could produce plumes with densities low enough that they would not collapse. It cannot be entirely excluded that some relatively small PDCs did form, but that their deposits are not preserved. It seems unlikely, however, that major PDC deposits would not have left any trace in the stratigraphic record, while the RP fall deposit is overall relatively well-preserved. The fact that no caldera was formed suggests that the Rungwe magma chamber is located at least a few km beneath the surface.

A relatively high MDR is, in the case of RP, probably associated with a high magmatic volatile content (especially CO_2, H_2O, F and Cl), as expected for alkaline melts. The few rheological data that exist for alkaline silicic magmas (i.e. phonolite, trachyte) suggest that the water solubility in trachytic magmas is much higher than in e.g. rhyolite magmas, and that the solubility also increases with increasing Na content (Di Matteo et al. 2004). Whole-rock compositions for RP pumices (Fontijn et al. 2010b) show Na_2O contents of 5–6 wt%. Di Matteo et al. (2004) conclude that water-saturated trachytic magmas can still contain large amounts of dissolved water upon eruption. A high volatile content not only is associated with a constant high MDR but also explains the low density and hence high vesicularity of pumices, on the order of 80–85%.

The available field data only sample the high-Re particles falling in a turbulent regime from the umbrella cloud (Fig. 8). This limited exposure has implications for estimates of several eruptive parameters, because the fine grain sizes are usually not incorporated. The volume of 3.2–5.8 km^3 and mass of $1.1–2.0\times10^{12}$ kg (Table 1) are likely underestimates of the actual original volume and mass

deposited during the eruption. Where only proximal-medial umbrella-cloud deposition is preserved in the geological record for a Plinian eruption, models show that estimated volume can greatly underestimate the true deposit volume (Bonadonna et al. 1998), so that it is anticipated that the Rungwe eruption magnitude may be underestimated by a minimum factor of 2 due to poor preservation in distal areas. Underrepresentation of the fine fraction also implies a TGSD that is biased towards the coarse grain sizes, although how much so is difficult to quantify because inaccessibility of proximal deposits (within Rungwe crater and on Rungwe's steep and densely forested flanks) also leads to an unquantified underrepresentation of the coarse fraction. The TGSDs obtained with four different methods ("Total grain size distribution" section, Fig. 6, Table 1) yield Md_ϕ values which are generally lower (i.e. coarser) and σ_ϕ values which are generally lower (i.e. better sorted) than the very few other TGSD datasets available for Plinian eruptions (e.g. Durant et al. 2009; Volentik et al. 2010).

Exposure of only the coarse-grained medial part of the deposit also explains why no break-in-slope is seen on the thinning plot if the Lake Malawi data point is not considered (Fig. 7). Application of the model of Bonadonna and Phillips (2003) suggests a break-in-slope associated with the transition from the turbulent- to intermediate-dominant "umbrella" sedimentation regime (Segment 1 to Segment 2; Bonadonna et al. 1998) at 40–60 km and a break-in-slope associated with the transition from the intermediate to the laminar sedimentation regime (Segment 2 to Segment 3; Bonadonna et al. 1998) at ca. 100-km distance along the dispersal axis (Fig. 8). This distance of the Segment 2/Segment 3 break-in-slope corresponds to an $\sqrt{A}$ of ca. 125 km suggesting that the Lake Malawi data point belongs to Segment 3, i.e. the laminar sedimentation regime (Fig. 7).

From the accumulation per unit distance data in function of distance from the vent (Fig. 9), we can infer that a slight dispersal to the South-East occurred during the eruption, confirming the slightly elliptical contour patterns seen on isopach, isomass and isopleth maps (Figs. 3 and 4a). The plume corner position along the South-Eastern axis is estimated at ca. 12-km distance from the vent (i.e. the centre of the summit crater depression), whereas it was estimated at ca. 10.5 km along the Southern axis (Fig. 9) and between 8.5 and 11.5 km along the Eastern axis (Table 1).

The accumulation pattern shown by particles 16–32 and 8–16 mm is the result from fallout from the plume margins. The 8–16-mm grain size class is probably sedimented in a transitional regime, especially along the Southern axis (Fig. 9). Particles 4–8 mm down to 1–2 mm show a maximum in accumulation per unit distance reflecting the plume corner position, and this pattern is interpreted as the result from fallout from the umbrella region of the plume.

Conclusions

The comprehensive documentation of what is preserved and accessible to observation for the RP deposit enables us to estimate crucial eruptive parameters. Based on empirical modelling, the maximum eruption column height is estimated as 30.5–35 km, corresponding to a peak MDR of 2.8–4.8×10^8 kg/s. Inversion of TEPHRA2 on grain size results in H_T 33±4 km associated with an average MDR of 2.3–6.0×10^8 kg/s. The estimated TGSD of the exposed deposit part shows values for Md_ϕ of −1.5φ to −2.4φ and for σ_ϕ of 1.7–2.0. The model of Bonadonna and Phillips (2003) confirms that the exposed part of the deposit (ca. 7–30 km from the vent) is associated with the turbulent sedimentation regime. As a result, the Lake Malawi core data (ca. 115 km South-South-East from the vent) were crucial to constrain the thinning characteristics of the deposits better than would be possible using outcrops alone. The best estimate for the deposit volume, based on both empirical (exponential and power-law fit) and analytical calculations (TEPHRA2 inversion), is 3.2–5.8 km^3 corresponding to an erupted mass of 1.1–2.0×10^{12} kg (accounting for the Lake Malawi distal point). The RP clearly classifies as a Plinian eruption, with an inferred VEI 5 and magnitude 5–5.3, and serves as a rare case study of an eruption happening in nearly no-wind conditions. The plume corner distance was estimated at ca. 11–12 km. A second unique feature of the RP eruption is the lack of major PDCs and therefore of a significant plume collapse, probably due to the extremely low clast density of order 400–450 kg/m^3.

Acknowledgements KF and GGJE are supported by the Belgian Research Foundation (FWO-Vlaanderen). Damien Delvaux is acknowledged for introduction in the field and providing assistance in obtaining working permissions. Edista Abdallah, Shimba Kwelwa, Shaban Sangalala, Gabriel Mwakyambiki and the people from Bongo Camping in Kibisi-Tukuyu are acknowledged for their support and friendship during and after field work. Danielle Schram is highly acknowledged for assistance with grain size analyses. Toon Van Dijck is thanked for assisting in pumice density measurements, and Alain Volentik for sharing thickness data from the Pululagua BF2 deposit. Reviews by Sebastian Watt and Mauro Rosi were highly appreciated and have improved the manuscript.

References

Barker P, Williamson D, Gasse F, Gibert E (2003) Climatic and volcanic forcing revealed in a 50,000-year diatom record from Lake Massoko, Tanzania. Quat Res 60:368–376

Barker PA, Leng MJ, Gasse F, Huang Y (2007) Century-to-millennial scale climatic variability in Lake Malawi revealed by isotope records. Earth Planet Sci Lett 261:93–103

Barry SL, Filippi ML, Talbot MR, Johnson TC (2002) Sedimentology and geochronology of Late Pleistocene and Holocene sediments from Northern Lake Malawi. In: Odada EO, Olaga DO (eds) The East African great lakes: limnology, palaeolimnology and

biodiversity. Kluwer Academic Publishers, Dordrecht, pp 369–391

Bonadonna C, Houghton BF (2005) Total grain size distribution and volume of tephra-fall deposits. Bull Volcanol 67:441–456

Bonadonna C, Phillips JC (2003) Sedimentation from strong volcanic plumes. J Geophys Res 108:2340. doi:10.1029/2002JB002034

Bonadonna C, Ernst GGJ, Sparks RSJ (1998) Thickness variations and volume estimates of tephra fall deposits: the importance of particle Reynolds number. J Volcanol Geotherm Res 81:173–187

Bonadonna C, Connor CB, Houghton BF, Connor L, Byrne M, Laing A, Hincks TK (2005) Probabilistic modeling of tephra dispersal: hazard assessment of a multiphase rhyolitic eruption at Tarawera, New Zealand. J Geophys Res 110:B03203. doi:10.1029/2003JB002896

Bursik MI, Sparks RSJ, Gilbert JS, Carey SN (1992) Sedimentation of tephra by volcanic plumes: I. Theory and its comparison with a study of the Fogo A Plinian deposit, Sao Miguel (Azores). Bull Volcanol 54:329–344

Carey SN, Sigurdsson H (1989) The intensity of Plinian eruptions. Bull Volcanol 51:28–40

Carey S, Sparks RSJ (1986) Quantitative models of the fallout and dispersal of tephra from volcanic eruption columns. Bull Volcanol 48:109–125

Cas RAF, Wright JV (1987) Volcanic successions, modern and ancient: a geological approach to processes, products and successions. Unwin Hyman Ltd, London

Connor LJ, Connor CB (2006) Inversion is the key to dispersion: understanding eruption dynamics by inverting tephra fallout. In: Mader H, Coles SG, Connor CB, Connor LJ (eds) Statistics in volcanology. Geological Society, London, pp 231–242

Delvaux D (2001) Tectonic and palaeostress evolution of the Tanganyika-Rukwa-Malawi rift segment, East African rift System. In: Ziegler PA, Cavazza W, Robertson AHF, Crasquin-Soleau S (eds), PeriTethyan Rift/Wrench Basins and Passive Margins, Mem Mus Natl Hist Nat, PeriTethys Mem 6, Paris

Delvaux D, Levi K, Kajara R, Sarota J (1992) Cenozoic palaeostress and kinematic evolution of the Rukwa-North Malawi rift valley (East African Rift System). Bull Cent Rech Explor-Prod Elf Aquitaine 16:383–406

Di Matteo V, Carroll MR, Behrens H, Vetere F, Brooker RA (2004) Water solubility in trachytic melts. Chem Geol 213:187–196

Durant AJ, Rose WI, Sarna-Wojcicki AM, Carey S, Volentik ACM (2009) Hydrometeor-enhanced tephra sedimentation: constraints from the 18 May 1980 eruption of Mount St. Helens (USA). J Geophys Res 114:B03204. doi:10.1029/2008JB005756

Ebinger CJ, Deino AL, Drake RE, Tesha AL (1989) Chronology of volcanism and rift basin propagation—Rungwe Volcanic Province, East Africa. J Geophys Res 94:15785–15803

Ebinger CJ, Deino AL, Tesha AL, Becker T, Ring U (1993) Tectonic controls on rift basin morphology—evolution of the northern Malawi (Nyasa) Rift. J Geophys Res 98:17821–17836

Fontijn K, Delvaux D, Ernst GGJ, Mbede E, Jacobs P (2010a) Tectonic control over active volcanism at a range of scales: case of the Rungwe Volcanic Province, SW Tanzania; and hazard implications. J Afr Earth Sci 58:764–777

Fontijn K, Ernst GGJ, Elburg MA, Williamson D, Abdallah E, Kwelwa S, Mbede E, Jacobs P (2010b) Holocene explosive eruptions in the Rungwe Volcanic Province, Tanzania. J Volcanol Geotherm Res 196:91–110

Harkin DA (1960) The Rungwe volcanics at the northern end of Lake Nyasa. Mem Geol Surv Tanganyika 11

Hildreth W, Drake RE (1992) Volcán Quizapu, Chilean Andes. Bull Volcanol 54:93–125

IAVCEI Commission on Tephra Hazard Modelling (2006) Field measurements for the characterization of tephra deposits. Field workshop report, Ecuador, 16–18 January 2006, 48 pp, http://www.ct.ingv.it/Progetti/Iavcei/report1.htm. Accessed 15 July 2010

Inman DL (1952) Measures for describing the size distribution of sediments. J Sed Petrol 22:125–145

Johnson TC, Brown ET, McManus J, Barry S, Barker P, Gasse F (2002) A high-resolution paleoclimate record spanning the past 25,000 years in Southern East Africa. Science 296(113–114): 131–132

Johnson TC, Brown ET, Shi J (2010) Biogenic silica deposition in Lake Malawi, East Africa over the past 150,000 years. Palaeogeogr Palaeocl. doi:10.1016/j.palaeo.2010.01.024

Kaminski E, Jaupart C (1998) The size distribution of pyroclasts and the fragmentation sequence in explosive volcanic eruptions. J Geophys Res 103:29759–29779

Newhall CG, Punongbayan RS (1996) Fire and mud: eruptions and lahars of Mount Pinatubo, Philippines. University of Washington Press, London

Newhall CG, Self S (1982) The Volcanic Explosivity Index (VEI)—an estimate of explosive magnitude for historical volcanism. J Geophys Res 87:1231–1238

Papale P, Rosi M (1993) A case of no-wind Plinian fallout at Pululagua caldera (Ecuador): implications for models of clast dispersal. Bull Volcanol 55:523–535

Polacci M, Pioli L, Rosi M (2003) The Plinian phase of the Campanian Ignimbrite eruption (Phlegrean Fields, Italy): evidence from density measurements and textural characterization of pumice. Bull Volcanol 65:418–432

Polacci M, Papale P, Del Seppia D, Giordano D, Romano C (2004) Dynamics of magma ascent and fragmentation in trachytic versus rhyolitic eruptions. J Volcanol Geotherm Res 131:93–108

Pyle DM (1989) The thickness, volume and grainsize of tephra fall deposits. Bull Volcanol 51:1–15

Pyle DM (1995) Assessment of the minimum volume of tephra fall deposits. J Volcanol Geotherm Res 69:379–382

Pyle DM (1999) Widely dispersed quaternary tephra in Africa. Global Planet Change 21:95–112

Pyle DM (2000) Sizes of volcanic eruptions. In: Sigurdsson H, Houghton B, Rymer H, Stix J, McNutt SR (eds) Encyclopedia of volcanoes. Academic Press, pp 263–269

Ring U, Betzler C, Delvaux D (1992) Normal vs. strike-slip faulting during rift development in East Africa: the Malawi rift. Geology 20:1015–1018

Sarna-Wojcicki AM, Shipley S, Waitt RB, Dzurisin D, Wood SH (1981) Areal distribution, thickness, mass, volume, and grain size of air-fall ash from the six major eruptions of 1980. In: Lipman PW, Mullineaux DR (eds) The 1980 eruptions of Mount St Helens, Washington. USGS Prof Paper 1250:577–600

Scasso R, Corbella H, Tiberi P (1994) Sedimentological analysis of the tephra from 12–15 August 1991 eruption of Hudson volcano. Bull Volcanol 56:121–132

Siebert L, Simkin T, Kimberly P (2011) Volcanoes of the world, 3rd edn. The University of California Press, Berkeley

Sparks RSJ (1986) The dimensions and dynamics of volcanic eruption columns. Bull Volcanol 48:3–15

Sulpizio R (2005) Three empirical methods for the calculation of distal volume of tephra-fall deposits. J Volcanol Geotherm Res 145:315–336

Thevenon F, Williamson D, Taieb M (2002) A 22 kyr BP sedimentological record of Lake Rukwa (8°S, SW Tanzania): environmental, chronostratigraphic and climatic implications. Palaeogeogr Palaeocl 187:285–294

Thorarinsson S (1954) The tephra-fall from Hekla on March 29th 1947. The eruption of Hekla 1947–48(2):1–68

United Republic of Tanzania (2002) Population and Housing Census. National Bureau of Statistics. http://www.nbs.go.tz. Accessed 5 February 2010.

USGS (2006) Shuttle radar topography mission. 3 arc second scene 179–057, filled finished-B. Global land cover facility. University of Maryland, Maryland

Volentik ACM, Bonadonna C, Connor CB, Connor LJ, Rosi M (2010) Modeling tephra dispersal in absence of wind: Insights from the climactic phase of the 2450 BP Plinian eruption of Pululagua volcano (Ecuador). J Volcanol Geotherm Res 193:117–136

Walker GPL (1971) Grain-size characteristics of pyroclastic deposits. J Geol 79:696–714

Walker GPL (1973) Explosive volcanic eruptions—a new classification scheme. Geol Rundsch 62:431–446

Walker GPL (1981) Characteristics of two phreatoplinian ashes, and their water-flushed origin. J Volcanol Geotherm Res 9:395–407

Williams SN, Self S (1983) The October 1902 plinian eruption of Santa María Volcano, Guatemala. J Volcanol Geotherm Res 16:33–56

Williams TM, Henney PJ, Owen RB (1993) Recent eruptive episodes of the Rungwe Volcanic Field (Tanzania) recorded in lacustrine sediments of the northern Malawi rift. J Afr Earth Sci 17:33–39

Wilson L, Walker GPL (1987) Explosive volcanic eruptions-VI. Ejecta dispersal in Plinian eruptions: the control of eruption conditions and atmospheric properties. Geophys J Roy Astr Soc 89:657–679

Woods AW (1998) Observations and models of volcanic eruption columns. In: Gilbert JS, Sparks RSJ (eds) The physics of explosive volcanic eruptions. Geol Soc Spec Publ 145:91–114

Woods AW, Bower SM (1995) The decompression of volcanic jets in a crater during explosive volcanic eruptions. Earth Planet Sci Lett 131:189–205